
# Proton-transport catalysis, proton abstraction, and proton exchange in HF+HOC + and H 2 O+HOC + and analogous deuterated reactions

Michael A. Collins and Leo Radom

Citation: The Journal of Chemical Physics **118**, 6222 (2003); doi: 10.1063/1.1559480
View online: http://dx.doi.org/10.1063/1.1559480
View Table of Contents: http://scitation.aip.org/content/aip/journal/jcp/118/14?ver=pdfcov
Published by the AIP Publishing

**Articles you may be interested in**

Probes of spin conservation in heavy metal reactions: Experimental and theoretical studies of the reactions of Re + with H 2 , D 2 , and HD
J. Chem. Phys. **121**, 248 (2004); 10.1063/1.1758695

Inclusion of quantum-mechanical vibrational energy in reactive potentials of mean force
J. Chem. Phys. **114**, 9953 (2001); 10.1063/1.1371497

Proton-transport catalysis and proton-abstraction reactions: An ab initio dynamical study of X+HOC + and XH + + CO (X=Ne, Ar, and Kr)
J. Chem. Phys. **112**, 6625 (2000); 10.1063/1.481235

A direct-dynamics study of proton transfer through water bridges in guanine and 7-azaindole
J. Chem. Phys. **112**, 566 (2000); 10.1063/1.480549

Ab initio study on the mechanism of C 2 H 2 + +NH 3 reaction: Efficient charge transfer and proton transfer processes competing with stable complex formation
J. Chem. Phys. **108**, 4021 (1998); 10.1063/1.476230


This article is copyrighted as indicated in the article. Reuse of AIP content is subject to the terms at: http://scitation.aip.org/termsconditions. Downloaded to IP: 130.56.106.27 On: Mon, 12 Oct 2015 04:33:38

# Proton-transport catalysis, proton abstraction, and proton exchange in $HF+HOC^+$ and $H_2O+HOC^+$ and analogous deuterated reactions

Michael A. Collins[a] and Leo Radom
*Research School of Chemistry, Australian National University, Canberra, ACT 0200, Australia*

(Received 11 November 2002; accepted 21 January 2003)

Classical simulations of the reactions of HF and $H_2O$ with $HOC^+$ have been carried out on interpolated *ab initio* potential energy surfaces. Rearrangement ($X+HOC^+ \rightarrow OCH^+ + X$), abstraction ($X+HOC^+ \rightarrow XH^+ + OC$), (X=HF or $H_2O$), exchange (e.g., $DY+HOC^+ \rightarrow HY+DOC^+$), and exchange-rearrangement (e.g., $DY+HOC^+ \rightarrow OCD^+ + YH$) (Y=F or HO or DO) reactions are observed. However, the abstraction reaction is dominant for both the $HF+HOC^+$ and $H_2O+HOC^+$ systems. © *2003 American Institute of Physics.* [DOI: 10.1063/1.1559480]

## I. INTRODUCTION

There is a substantial barrier of about 160 kJ $mol^{-1}$ separating the isoformyl cation ($HOC^+$) from its much more stable isomer, the formyl cation ($OCH^+$).[1–11] While the isolated isoformyl cation is relatively stable,[8–10,12–17] the barrier for the rearrangement of $HOC^+$ to $OCH^+$ is substantially reduced, or in some cases even eliminated, during a collision with an appropriate neutral molecule (X).[1,10,11,14,18] This is an example of what Bohme has described as catalyzed proton transport,[19] or what may be referred to more generally as ion-transport catalysis.[20]

The proton affinity of the collider (X) is important because complexation of X with $HOC^+$ weakens the H···O bond, thus facilitating the rearrangement,[18]

$$X+HOC^+ \rightarrow [XH\cdots OC]^+ \rightarrow [OC\cdots HX]^+ \rightarrow OCH^+ + X. \tag{1.1}$$

A systematic theoretical study,[18] found that when X has a proton affinity less than that of CO at either O or C (e.g., X=He, Ne, and Ar), the barrier to rearrangement is reduced but not eliminated. In cases where X has a proton affinity lying between that of CO at O and C (e.g., X=HF), the barrier disappears. Finally, for molecules X with a proton affinity greater than that of CO at O or C (e.g., X=$H_2O$), the barrier for rearrangement also disappears, but in such cases an alternative reaction, hydrogen abstraction, is energetically preferred,

$$X+HOC^+ \rightarrow XH^+ + OC. \tag{1.2}$$

In a recent paper,[21] we examined the dynamical consequences of lowering but not eliminating the barrier to rearrangement in collisions of $HOC^+$ with three rare gases (X =Ne, Ar, and Kr). *Ab initio* potential energy surfaces (PESs) were constructed for each collider, and classical trajectory studies of the collisions were carried out. For $Ne+HOC^+$, the barrier to rearrangement is very high and rearrangement is thus impractical. However, for $Ar+HOC^+$, and particularly for $Kr+HOC^+$, the barrier is sufficiently low that cross sections for the rearrangement reaction could be evaluated. Interestingly, it was found that once the collision energy is sufficiently high for the abstraction reaction (1.2) to be feasible, this process competes with and dominates the energetically-preferred rearrangement reaction (1.1).

In this paper, we examine the collision of $HOC^+$ with HF and $H_2O$ where the rearrangement and abstraction reactions are expected to be more facile on energetic grounds. There is also the possibility of additional reactions, namely, the exchange (1.3 and 1.4) and exchange-rearrangement (1.5 and 1.6) reactions (Y=F or HO or DO),

$$DY+HOC^+ \rightarrow HY+DOC^+, \tag{1.3}$$

$$HY+DOC^+ \rightarrow DY+HOC^+, \tag{1.4}$$

$$DY+HOC^+ \rightarrow OCD^+ + YH, \tag{1.5}$$

$$HY+DOC^+ \rightarrow OCH^+ + YD. \tag{1.6}$$

In order to examine theoretically the competition between reactions (1.1)–(1.6), global *ab initio* PESs have been constructed for $HF+HOC^+$ and $H_2O+HOC^+$ using interpolation methods.[22–27] The construction of potential energy surfaces for these two systems represents a very demanding task for a number of reasons. First, there are three asymptotic channels in these systems (including the reactants) and there is the possibility of complicated motion involved in exchange, so that the range of molecular configurations that must be described is large. Second, the energy range involved in these ion–molecule reactions is also relatively large. Finally, when this work was initiated, there had been no previous attempts to construct completely *ab initio* global potential energy surfaces for systems of more than four atoms, although subsequently an interpolated PES has been constructed for triazine at the B-LYP level of theory.[28]

The paper is constructed as follows: Section II briefly reviews the results of an earlier *ab initio* study[18] that formed the basis for choosing the electronic structure approach. Here, we also briefly describe the interpolation method and iterative scheme used to construct the PES from the *ab initio* calculations. Section III presents our results including the basic topology of the PESs as described by the minimum energy paths for these reactions, the classical cross sections for reactions (1.1)–(1.6), and mechanistic information for

[a]Electronic mail: collins@rsc.anu.edu.au

 © 2003 American Institute of Physics

This article is copyrighted as indicated in the article. Reuse of AIP content is subject to the terms at: http://scitation.aip.org/termsconditions. Downloaded to IP: 130.56.106.27 On: Mon, 12 Oct 2015 04:33:38

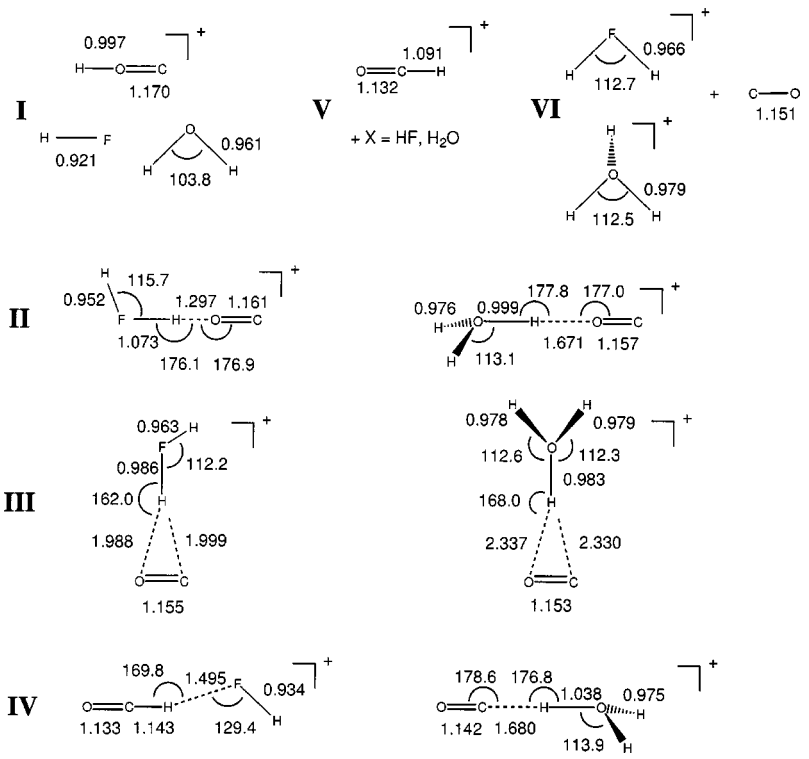


FIG. 1. Schematic representation of stationary points on the potential energy surfaces for $[HFHOC]^+$ and $[H_2OHOC]^+$. The geometries have been optimized at the MP2/6-31G** level of theory.

these reactions that comes from a consideration of the energy distributions in the products and other quantities obtained from the trajectory simulations. Section IV presents some concluding remarks.

## II. POTENTIAL ENERGY SURFACES

### A. Levels of *ab initio* theory

The *ab initio* PES calculations reported herein have been carried out using the GAUSSIAN 94 and GAUSSIAN 98 suites of programs[29,30] and have employed spin-restricted (R) formalisms.

A previous systematic *ab initio* study of the $[HFHOC]^+$, $[H_2OHOC]^+$, and related systems[18] showed that the MP2/6-31G** level of theory predicts the geometries of the various stationary points on the PES to reasonable accuracy. These optimized geometries are displayed in Fig. 1. Accurate evaluation of the energies of these stationary points requires higher levels of theory, and a modification of the composite G2 method, termed G2**, was found to be appropriate in this regard.[18] Although the energies of stationary points for $[HFHOC]^+$ and $[H_2OHOC]^+$ at the MP2/6-31G** level of theory can differ from the values given by G2** calculations by tens of kJ mol$^{-1}$ (see Table I), the energy range of these features on the PES is sufficiently large (about 270 kJ mol$^{-1}$ for $[HFHOC]^+$ and about 360 kJ mol$^{-1}$ for $[H_2OHOC]^+$ that the MP2/6-31G** surfaces are adequate approximations to the exact PES. We note that the MP2/6-31G** relative energies of the stationary points in Table I reproduce the G2** results quite well, except that the relative energy of the $COH^+$ reactant is too high at the lower level of theory. Since construction of each PES requires evaluation of the energy gradients and second derivatives at more than 1000 configurations for these systems, we have adopted MP2/6-31G** as a suitable compromise level for the computations for $[HFHOC]^+$ and $[H_2OHOC]^+$. Since both of these ion–molecule reactions are barrierless, it is likely that the *total* reaction cross sections are mainly determined by the long range attractive forces between the reactants, rather than the relative energies of the reactants and products. The overestimate of the energy of the $COH^+$ reactant will lead to a higher energy available to the products than would be the case at the G2** level of theory.

### B. Form of the potential energy surface

The detailed formulation of the interpolated PES for systems of more than four atoms has been presented

TABLE I. Calculated relative energies (kJ mol$^{-1}$) for stationary points on the $[HFHOC]^+$ and $[H_2OHOC]^+$ potential energy surfaces.

| Species | MP2/6-31G** | MP2/6-31G** [a] | G2** [a,b] |
|---|---|---|---|
| HF+HOC$^+$ | 0 | 0 | 0 |
| HF···H···OC$^+$ | −177 | −169 | −132 |
| TS (III) | −113 | −107 | −69 |
| OC···H···FH$^+$ | −278 | −267 | −224 |
| OCH$^+$+FH | −188 | −180 | −158 |
| $H_2F^+$+OC | −93 | −89 | −50 |
| $H_2O$+HOC$^+$ | 0 | 0 | 0 |
| $H_2O$···H···OC$^+$ | −340 | −321 | −288 |
| TS (III) | −309 | −294 | −258 |
| OC···H···$OH_2^+$ | −373 | −355 | −312 |
| OCH$^+$+$OH_2$ | −188 | −180 | −158 |
| $H_3O^+$+OC | −300 | −287 | −252 |

[a]Including zero-point vibrational energies.
[b]From Ref. 18.

This article is copyrighted as indicated in the article. Reuse of AIP content is subject to the terms at: http://scitation.aip.org/termsconditions. Downloaded to IP: 130.56.106.27 On: Mon, 12 Oct 2015 04:33:38

previously,[23,26,27,31] and a recent review[32] provides a more concise exposition, so only a brief description is presented here.

The PES is given by a weighted average of Taylor expansions centered at data points scattered throughout the configuration space of the system,[22–27]

$$V=\sum_{g\in G}\sum_{i=1}^{N_{\rm data}} w_{g\circ i}T_{g\circ i}\,. \tag{2.1}$$

The second-order Taylor expansion, $T_i$, is assigned a weight, $w_i$, that gives the contribution of the $i$th Taylor expansion to the potential energy at each molecular configuration. In Eq. (2.1), $G$ denotes the symmetry group of the molecule, here the complete nuclear permutation inversion (CNPI) group, and $g\circ i$ denotes that the $i$th data point is transformed by the group element $g$. The sum over $g\in G$ means that all permutationally-equivalent data points are included in the data set, the energy derivatives at permuted data points being simple permutations of the original derivatives at each of the $N_{\rm data}$ geometries where *ab initio* calculations were performed. The data set is ''symmetrized,'' so that the PES of Eq. (2.1) exhibits the full molecular symmetry. The form of the Taylor expansion[26] and that of the weight function[27] have been described elsewhere. The weight function uses confidence lengths that were evaluated using an energy tolerance, $E_{\rm tol}=0.52$ kJ mol$^{-1}$, and energy gradients at $M$ data points ($M=36$ for $[{\rm HFHOC}]^+$ and $M=72$ for $[{\rm H_2OHOC}]^+$, see Ref. 27 for definitions of $E_{\rm tol}$ and $M$).

### C. Iterative development of the PES

The location of the data points in Eq. (2.1) has been determined using the iterative methods developed previously.[22,23,26] In summary, an initial set of data points is chosen to lie on or near the paths for reactions (1.1) and (1.2), the latter being obtained simply by minimizing the molecular energy (using GAUSSIAN 94 or GAUSSIAN 98) beginning at the asymptotic configurations and the known[18] saddle-points, structures III of Fig. 1. An initial data set of geometries (106 for $[{\rm HFHOC}]^+$ and 101 for $[{\rm H_2OHOC}]^+$) is selected from these minimizations. The potential of Eq. (2.1) is then well-defined in the vicinity of the reaction paths. Classical trajectories are evaluated, with initial conditions appropriate to the reactants, to explore the relevant region of configuration space. Molecular configurations encountered during these trajectories are recorded, and one or more of these configurations are then chosen to be a new data point. The *ab initio* energy, gradient and second derivatives are evaluated at that point which is added to the data set, generating a new version of the PES. This process of simulating the reaction(s), choosing a configuration, performing the *ab initio* calculations and adding a new data point to the set is repeated again and again until the PESs are ''converged.'' Convergence is established by performing large-scale classical simulations of the reaction(s) of interest and evaluating the reaction cross sections for surfaces with an increasing number of data points. Once the values of the reaction cross sections do not change significantly with increasing size of the data set, the PESs are taken to be converged.

The methods for choosing a new data point at each iteration have been discussed in detail elsewhere.[26] The ''variance sampling'' method places data points at configurations where the uncertainty in Eq. (2.1) is highest. The ''$h$ weight'' method attempts to place data in regions where the trajectories often visit, but where few data points are already present. Both ''variance sampling'' and ''$h$ weight'' methods were employed.

### D. Computational details

All classical trajectories performed, both during the iterative construction of the PES and to evaluate the scattering dynamics, were carried out using the standard methods previously detailed.[23–26] A step size of $1-2.5\times10^{-17}$ s was used in the velocity-Verlet integration algorithm.[33] Because of the long-range ion–dipole interaction between the reactants, the reactants were initially separated by 25.4 Å (48 $a_o$). Trajectories were terminated when any bond length exceeded the initial separation of the reactants while the molecular fragments were separating (rather than coming closer together). The maximum impact parameter was 3.6 Å (7 $a_o$) during the construction of the PESs, and 9.0 Å (17 $a_o$) for evaluation of reaction cross sections for $[{\rm HFHOC}]^+$ and 10.1 Å (19 $a_o$) for $[{\rm H_2OHOC}]^+$. Smaller impact parameters are used during the construction of the PESs to ensure that the molecular configurations encountered during the trajectories included close contact between the reactants. No type of molecular configuration is excluded by this approach, so that the PESs and resultant cross sections do not explicitly depend on the use of small impact parameters during the construction phase. All reactant molecules were given an initial microcanonical distribution of vibrational energy, for a total energy roughly approximating the value of the zero-point energy: 34.9 kJ mol$^{-1}$ for $HOC^+$, 28.2 kJ mol$^{-1}$ for $DOC^+$, 25.1 kJ mol$^{-1}$ for HF, 17.7 kJ mol$^{-1}$ for DF, 57.5 kJ mol$^{-1}$ for $H_2O$, and 40.7 kJ mol$^{-1}$ for $D_2O$. Random initial velocities and configurations for the atoms in each fragment were evaluated using the efficient microcanonical sampling method of Schranz *et al.*[34] The molecular fragments were initially randomly oriented and given zero rotational angular momentum, using a program also initially due to Schranz. The initial relative translational energy of the reactants was set to 13.1 kJ mol$^{-1}$ (5 mhartree) for all trajectories used in the construction of PESs and for evaluation of the cross sections. To ensure that the product regions of the surface were adequately explored during the iterative construction of the PES, trajectories were also evaluated with initial configurations corresponding to $XH^+ + OC$ and $X + OCH^+$ (X=HF or $H_2O$). The initial vibrational energy was taken to be 51.2 kJ mol$^{-1}$ for $FH_2^+$, 118.1 kJ mol$^{-1}$ for $H_3O^+$, and 17.8 kJ mol$^{-1}$ for CO.

For $HF+HOC^+$, the PES construction was iterated until the data set contained 1357 points. The twelve-dimensional PES for $H_2O+HOC^+$ was iteratively constructed until the data set contained 3047 points.

This article is copyrighted as indicated in the article. Reuse of AIP content is subject to the terms at: http://scitation.aip.org/termsconditions. Downloaded to IP: 130.56.106.27 On: Mon, 12 Oct 2015 04:33:38

### E. Accuracy of the interpolation

Some indication of the interpolation error remaining in the final PES can be gained from considering the average interpolation error in a sample of molecular configurations. A total of 1000 molecular configurations were generated by random sampling of configurations encountered in classical trajectories for $[HFHOC]^+$ and 828 configurations for $[H_2OHOC]^+$. The *ab initio* energy was evaluated at each configuration and compared with the value given by the interpolated PES. The final PESs have average interpolation errors, in these samples, of 1.5 and 3.5 kJ mol$^{-1}$, respectively. These average errors represent 0.45% and 0.81%, respectively, of the energy ranges of these sampled configurations. The average relative error for the $[H_2OHOC]^+$ PES is larger than that achieved for four-atom systems. However, interpolated PESs with a comparably high level of accuracy ($<1\%$ mean relative error) have been found to be sufficiently accurate to describe classical reaction rate coefficients.[35–38]

## III. RESULTS AND DISCUSSION

### A. Minimum energy paths

Figure 2 presents the energy profiles along the minimum energy paths for reactions (1.1) and (1.2), for X=Kr,[21] HF, and $H_2O$. These paths were obtained from the interpolated PES by following the paths of steepest descent in mass-weighted Cartesian coordinates that lead from various saddle points on the surface and from the asymptotic configurations. The reaction coordinate employed in the figures is a path length $S$, for which $dS=\|d\mathbf{R}\|$, where $\mathbf{R}$ is the vector of atom–atom distances. The arbitrary origins and directions for each segment of the path have been adjusted for pictorial convenience. The Roman numerals associate the stationary points on these paths with the corresponding geometries shown in Fig. 1. These three figures show that the barrier to rearrangement of HOC$^+$ (represented by the energies of structure III) lies above the energy of the entrance channel for collision with Kr but is lowered to a value below the energy of the entrance channel for collision with HF and lowered still further for collision with $H_2O$. In addition, the energy of the rearrangement product, OCH$^+$+X, is the lowest energy product for X=Kr and HF, but not for X=$H_2O$.

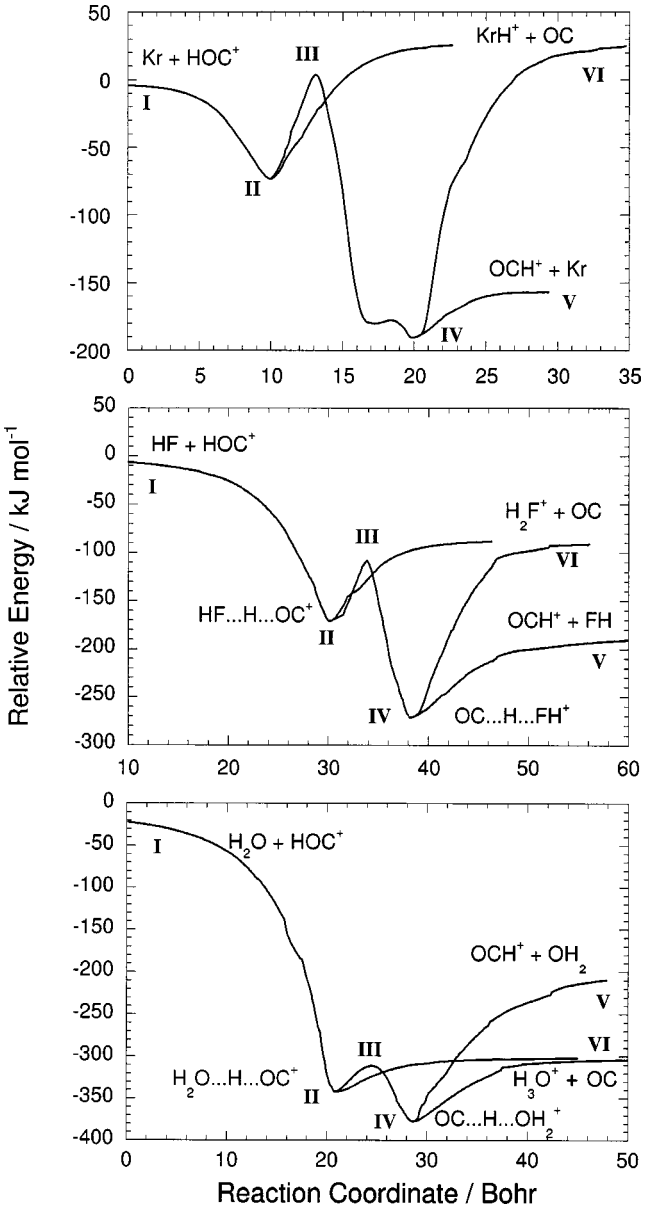


FIG. 2. The energy profiles along minimum energy paths on the $[HFHOC]^+$ and $[H_2OHOC]^+$ surfaces are compared with that for $[KrHOC]^+$ (see Ref. 21) as a function of a reaction coordinate (see text). The labeled stationary points are displayed in Fig. 1.

### B. Reaction cross sections

Table II presents the reaction cross sections, calculated from classical trajectories as described above. Ensembles of 1000 trajectories were employed for each reaction except for HF+DOC$^+$, where 2000 trajectories were evaluated. The convergence of the PESs was tested by comparing the cross sections with values obtained with fewer data points. For example, using data sets of 1357, 1257, and 1157 data points, respectively, the HF+COD$^+$ reaction produced the following cross sections (in Å$^2$, with estimated standard deviations): HFD$^+$+CO, 149±3, 150±4, 155±4; OCD$^+$+FH, 9±1, 10±1, 9±1; OCH$^+$+FD, 7±1, 8±1, 6±1; DF+HOC$^+$, (0.1), (0.5), (0.0). Similarly, using data sets of 3047, 2918, and 2767 data points, respectively, the $H_2O$+COH$^+$ reaction produced the following cross sections (Å$^2$): $H_3O^+$+CO, 210±5, 215±5, 218±5; OCH$^+$+$OH_2$, (0.3), (1.0), (1.0).

In every case, the cross section for hydrogen or deuterium abstraction is large. This is very likely due to a large ''capture'' cross section induced by the long-range ion–dipole interaction. Figure 3 shows the total probability of reactions (1.1)–(1.6) for HF+HOC$^+$ and $H_2O$+HOC$^+$ as a function of the impact parameter for the collision (the impact parameter is the initial displacement of the paths of the colliding molecules; it is the distance at which the reactants would pass by one another if there were no forces between them; it was calculated from the same trajectories as used to evaluate Table II). It is clear that a collision below some critical impact parameter leads to a reaction with near unit

This article is copyrighted as indicated in the article. Reuse of AIP content is subject to the terms at: http://scitation.aip.org/termsconditions. Downloaded to IP: 130.56.106.27 On: Mon, 12 Oct 2015 04:33:38

TABLE II. Total cross sections for products formed from the reactions of $HF+HOC^+$ and $H_2O+HOC^+$ and deuterated analogs.[a]

| Reactants | Products | Cross section (Å$^2$) |
|---|---|---|
| $HF+HOC^+$ | $H_2F^++OC$ | 157±4 |
| | $OCH^++FH$ | 11±2 |
| $DF+HOC^+$ | $DHF^++OC$ | 158±4 |
| | $OCH^++FD$ | 9±2 |
| | $OCD^++FH$ | 3±1 |
| | $HF+DOC^+$ | (0.8) |
| $HF+DOC^+$ | $HFD^++OC$ | 149±3 |
| | $OCD^++FH$ | 9±1 |
| | $OCH^++FD$ | 7±1 |
| | $DF+HOC^+$ | (0.1) |
| $H_2O+HOC^+$ | $H_3O^++OC$ | 210±5 |
| | $OCH^++OH_2$ | (0.3) |
| $D_2O+HOC^+$ | $D_2OH^++OC$ | 216±5 |
| | $OCH^++OD_2$ | (1.0) |
| | $OCD^++ODH$ | (0.6) |
| | $HDO+DOC^+$ | (0) |
| $H_2O+DOC^+$ | $H_2OD^++OC$ | 214±5 |
| | $OCD^++OH_2$ | (0.6) |
| | $OCH^++ODH$ | (1.6) |
| | $HDO+HOC^+$ | (0) |

[a]Error bars represent one standard deviation. Values in parentheses are too small to allow an estimate of the uncertainty.

efficiency, as would be expected for long-range capture and subsequent reaction without a barrier.

For the $[HFHOC]^+$ system, isomerization of $HOC^+$ (or $DOC^+$), reaction (1.1), is a significant minor pathway (see Table I). Rearrangement with exchange, reactions (1.5) and (1.6), has a somewhat smaller cross section but is still a significant minor pathway for the deuterated analogs of $HF+HOC^+$. These observations are consistent with collisions that are sufficiently ''long-lived'' to allow mixing or scrambling of the light, labile atoms. Inspection of individual trajectories verifies that such collisions are commonplace. However, simple ''direct'' collisions, in which the H or D atom is abstracted in a glancing collision, are also very common.

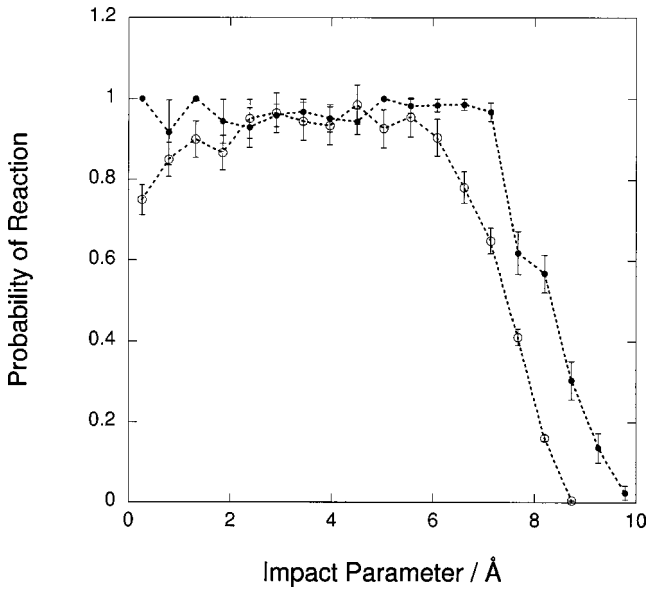


FIG. 3. The total probability of reactions (1.1)–(1.6) for $HF+HOC^+$ (●) and $H_2O+HOC^+$ (○) is shown as a function of the impact parameter for the collision. The relative frequencies were obtained with an impact parameter bin size of about 0.52 Å, and the error bars represent the estimated standard deviation of the probability of reactive trajectories as a fraction of all trajectories in the bin.

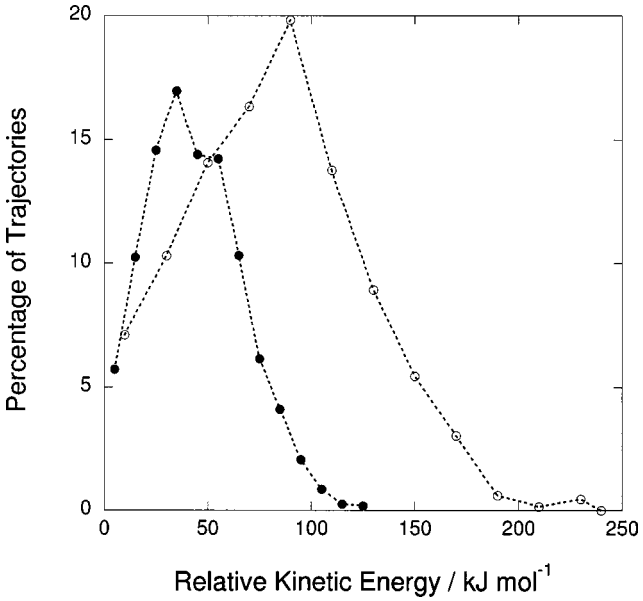


FIG. 4. The distribution for the relative kinetic energy of the separating abstraction products for $HF+DOC^+$ (●) and $H_2O+DOC^+$ (○). The relative frequencies were obtained with a bin size of 10 kJ mol$^{-1}$.

Direct abstraction is the overwhelmingly dominant process for the $[H_2OHOC]^+$ system. While both isomerization and arrangement with exchange are observed, the cross sections for both processes are lower by about an order of magnitude than for the corresponding reactions in the $[HFHOC]^+$ system, even though the total reaction cross section is larger. Simple exchange of the H or D atom at oxygen, reactions (1.3) and (1.4), was observed for the $[HFHOC]^+$ system, but not for the $[H_2OHOC]^+$ system (at least in 1000 trajectories).

In comparison, isomerization is the dominant process in $Kr+HOC^+$ collisions at low energy, where the abstraction channel is closed.[21] However, the reaction cross section for isomerization is only a few square angstroms. Abstraction becomes the major channel in this system when the energy is raised sufficiently for this process to be energetically allowed.

### C. Energy distributions and mechanism

In order to further investigate the mechanism of the abstraction reaction, it is useful to consider first the resultant distribution of energy and angular momentum in the products. Figure 4 presents the distribution of the relative kinetic energy of the separating abstraction products for $HF+DOC^+$ and $H_2O+DOC^+$. The mean relative kinetic energy is 44±23 kJ mol$^{-1}$ for the $HFD^+$ plus CO products, and 81±44 kJ mol$^{-1}$ for $H_2OD^+$ plus CO. This represents about 28% of the classically available energy for $HFD^+$ plus CO and about 20% for $H_2OD^+$ plus CO (see Table I and Sec. II D). Thus, while about 115 kJ mol$^{-1}$ of the total energy is

This article is copyrighted as indicated in the article. Reuse of AIP content is subject to the terms at: http://scitation.aip.org/termsconditions. Downloaded to IP: 130.56.106.27 On: Mon, 12 Oct 2015 04:33:38

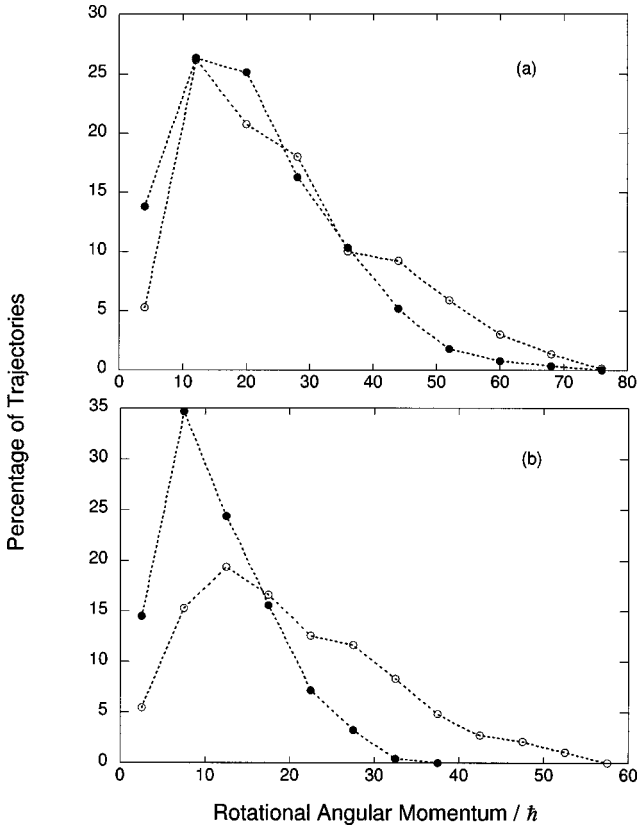


FIG. 5. The distribution of total rotational angular momentum in the abstraction products, (a) CO and (b) $HFD^+$ and $H_2OD^+$, is shown for HF+DOC$^+$ (●) and $H_2O$+DOC$^+$ (○). The relative frequencies were obtained with a bin size of 8 $\hbar$ in (a) and 5 $\hbar$ in (b).

directed towards vibration and rotation of the $HFD^+$ and CO products, about 319 kJ mol$^{-1}$ is directed to vibration and rotation of the $H_2OD^+$ and CO products. Figure 5 shows the distribution of rotational angular momentum in the abstraction products from the HF+DOC$^+$ and $H_2O$+DOC$^+$ collisions. Both abstraction products are more rotationally excited for the collision with $H_2O$ than with HF. The mean angular momentum for CO is 21 $\hbar$ for the $[HFHOC]^+$ system and 26 $\hbar$ for the $[H_2OHOC]^+$ system. Similarly, $HFD^+$ is produced with an average angular momentum of 11 $\hbar$, compared with 20 $\hbar$ for $H_2OD^+$.

It is natural to inquire whether the abstraction mechanism differs significantly between these two systems in such a way as to produce these differences in the product distributions. The reaction paths of Fig. 2 do not suggest any particular critical configuration for the abstraction process. The reaction occurs without a barrier in both cases, so there is no obvious transition state. As an alternative, we can ask what geometry has the breaking H···O bond in HOC$^+$ stretched to be the same length as the forming F···H or O···H bond in the protonated product? Figure 6 presents the distribution of lengths for the breaking H···O bond in HOC$^+$ when this length equals that of the forming bond (as calculated from an ensemble of reactive trajectories for both the $[HFHOC]^+$ and $[H_2OHOC]^+$ systems). The average length of the H···O bond is about 1.25±0.07 Å for the $[HFHOC]^+$ system and 1.34±0.08 Å for $[H_2OHOC]^+$. Two observations

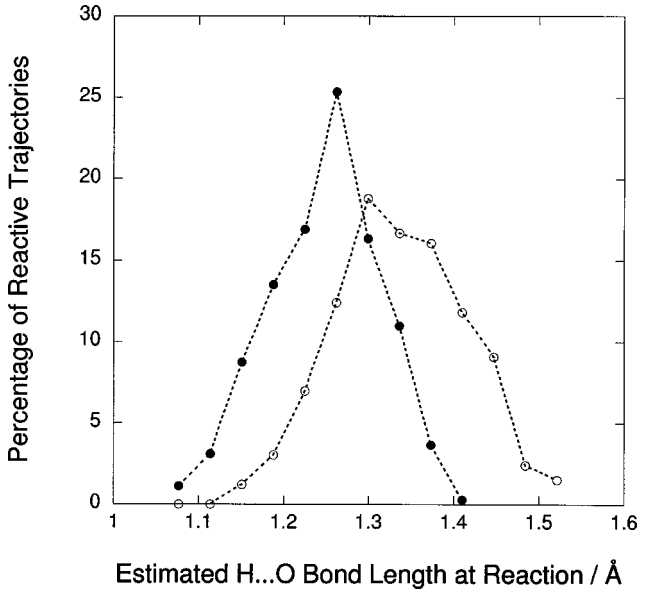


FIG. 6. The distribution of breaking H···O bond lengths (see text) in HF+HOC$^+$ (●) and $H_2O$+HOC$^+$ (○). The relative frequencies were obtained with a bin size of about 0.037 Å.

are apparent. First, according to this picture, the proton transfer to $H_2O$ occurs at slightly longer range than to HF. Second, the standard deviation of the bond length distributions is small in both systems. Apparently, the proton transfer is characterized by a relatively well defined bond length. Figure 7 shows the distribution of FHO angles (for $[HFHOC]^+$) and OHO angles (for $[H_2OHOC]^+$) corresponding to the same geometries as in Fig. 6. The average angles are about 160 ±13° in both cases. Since the probability distribution for a bond angle, $\theta$, with random atomic positions, is proportional

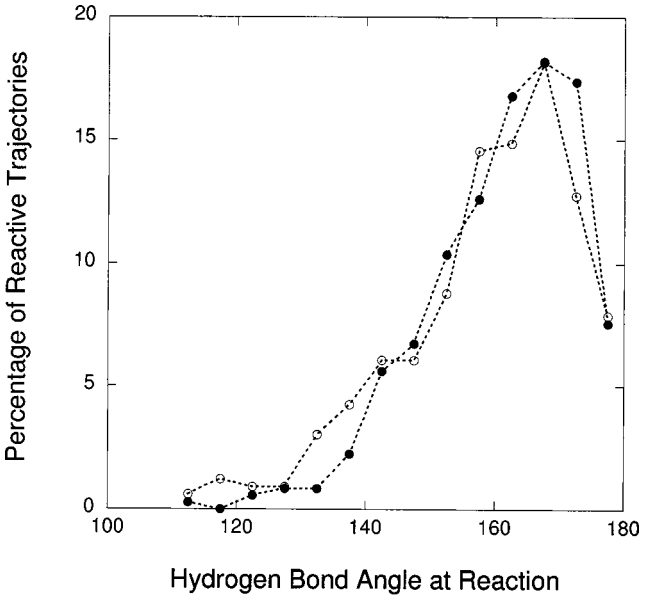


FIG. 7. The distribution of FHO and OHO bond angles (see text) in HF+HOC$^+$ (●) and $H_2O$+HOC$^+$ (○), respectively, for the same geometries as used in Fig. 6. The relative frequencies were obtained with a bin size of 5°.

This article is copyrighted as indicated in the article. Reuse of AIP content is subject to the terms at: http://scitation.aip.org/termsconditions. Downloaded to IP: 130.56.106.27 On: Mon, 12 Oct 2015 04:33:38

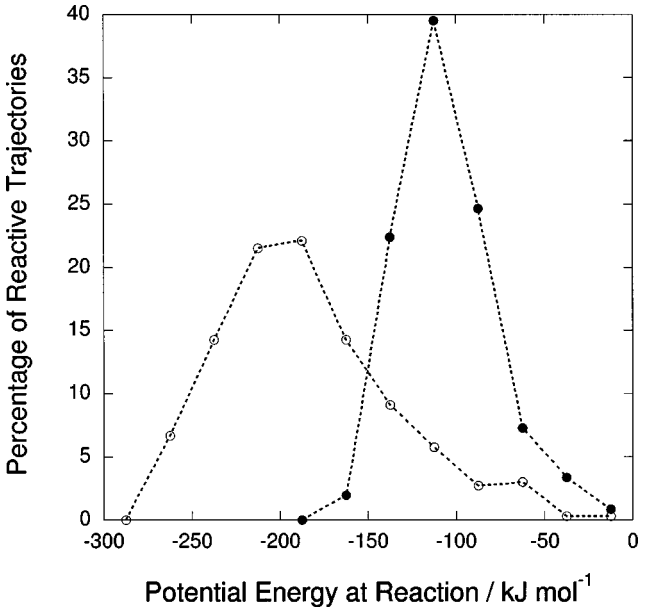


FIG. 8. The distribution of the potential energy in $HF+HOC^+$ (●) and $H_2O+HOC^+$ (○), respectively, calculated at the same geometries as used in Fig. 6. The relative frequencies were obtained with a bin size of 25 kJ mol$^{-1}$.

to sin($\theta$), it is clear that a near-collinear FHO or OHO geometry is strongly preferred at this ''point of proton transfer.''

The abstraction reaction thus appears to take place preferentially at near-collinear configurations with similar bond lengths in both systems. However, although the H···O bond lengths and FHO/OHO angles are fairly well defined at this ''bond-breaking'' configuration, there is a broad distribution of molecular configurations, as evidenced by the variation of the potential energy at this point of proton transfer, shown in Fig. 8. The mean potential energy for $[HFHOC]^+$ at these bond-breaking configurations is $-106\pm27$ kJ mol$^{-1}$. This mean energy is about 13 kJ mol$^{-1}$ below the equilibrium energy of the reaction products but about 71 kJ mol$^{-1}$ above the local minimum energy $[HF\cdots H\cdots OC]^+$ configuration. The corresponding mean potential energy is $-185\pm48$ kJ mol$^{-1}$ for $[H_2OHOC]^+$. This is about 115 kJ mol$^{-1}$ above the equilibrium energy of the reaction products and about 155 kJ mol$^{-1}$ above the local minimum energy $[H_2O\cdots H\cdots OC]^+$ configuration.

The optimized structures in Fig. 1 show that the proton in $HOC^+$ is closer to the acceptor, HF or $H_2O$, than to OC at the local minimum, $X\cdots H\cdots OC^+$ (II), in the entrance channel. Hence, we could reasonably view the ''point of proton transfer'' as residing in the entrance valley, on the reactant ''side'' of the minimum. For $[HFHOC]^+$, this point in the entrance valley lies below the energy of the separated products. Hence, it is reasonable to expect that there is a propensity for some temporary trapping of reactive trajectories in the ion–molecule complex. In contrast, the ''point of proton transfer'' lies higher in energy than the separated products for the $[H_2OHOC]^+$ system. The energy at this point is well above that of the minimum in the entrance valley, and at a longer O···H bond length than for $[HFHOC]^+$. Hence, although the average energy of the ''point of proton transfer'' is much lower in absolute terms for $[H_2OHOC]^+$ than for $[HFHOC]^+$, it is reasonable to describe proton transfer as taking place ''earlier'' in the entrance valley for $[H_2OHOC]^+$ than for $[HFHOC]^+$.

To investigate the duration of the collisions, we have evaluated the length of time that each trajectory spends with the two molecular fragments in close proximity. If $R_{close}$ is the average of the F···O and F···C separations in $[HFHOC]^+$ (or the corresponding O···O and O···C separations in $[H_2OHOC]^+$, then $T_{close}$ is (arbitrarily) defined to be the length of time for which $R_{close}<3.44$ Å (6.5 a.u.) during a trajectory. For ensembles of trajectories under the same conditions above, the average value of $T_{close}$ for trajectories leading to abstraction is 132 fs for $[HFHOC]^+$ and 84 fs for $[H_2OHOC]^+$. Moreover, for the $[H_2OHOC]^+$ system, $T_{close}=0$ for all nonreactive trajectories, while about 15% of nonreactive trajectories for $[HFHOC]^+$ were trapped for an average of 240 fs. Clearly, temporary trapping in the ion–molecule complex is a significant factor in the dynamics of $[HFHOC]^+$ but not of $[H_2OHOC]^+$.

The higher proton affinity of $H_2O$ compared with that of HF, is shown by the larger exothermicity of the abstraction reaction for $H_2O$. It is also plausible that this difference in proton affinity leads to proton transfer at a larger O···O distance than O···F distance and ''earlier'' in the entrance channel. As a consequence, proton transfer takes place above the energy of the products for the $[H_2OCOC]^+$ system, but below this energy for $[HFHOC]^+$. Part of the energy available from the reaction therefore produces a high relative velocity for the separating fragments of $[H_2OHOC]^+$, so that, without a barrier to surmount, the ion–molecule complex is short-lived or not formed in any meaningful sense. The exchange and isomerization reactions are therefore unlikely in $[H_2OHOC]^+$. For $[HFHOC]^+$, proton transfer takes place at a similar, slightly more compressed, geometry than it does for $[H_2OHOC]^+$, but at an energy below that of the separated products. Hence, we could characterize this location as within the ion–molecule well. Separation of the fragments is slightly impeded, sometimes long enough for isomerization and exchange processes to occur.

From this point of view, one might ask why the reaction products are more strongly internally excited for $[H_2OHOC]^+$ than for $[HFHOC]^+$. Without attempting a quantitative response to this question, it is useful to observe that (a) there are three more internal modes available for $[H_2OHOC]^+$; (b) the total energy available from the exothermicity of the reaction is very much larger for $[H_2OHOC]^+$; and (c) the more sudden proton transfer to $H_2O$ than to HF may result in higher excitation of the products than is the case for $[HFHOC]^+$. Some evidence for this suggestion is given by Fig. 8. The broad potential energy distribution for $[H_2OHOC]^+$ at the point of proton transfer might indicate that the structure of $[H_2O\cdots H]^+$ at the point of proton transfer is far from the equilibrium structure of $H_3O^+$. If so, one would expect a highly vibrationally excited $H_3O^+$ product.

## IV. CONCLUDING REMARKS

We have constructed *ab initio* molecular potential energy surfaces and carried out classical trajectory simulations to

This article is copyrighted as indicated in the article. Reuse of AIP content is subject to the terms at: http://scitation.aip.org/termsconditions. Downloaded to IP: 130.56.106.27 On: Mon, 12 Oct 2015 04:33:38

study proton rearrangement, proton abstraction, and proton exchange in the reaction $HF+HOC^+$ and $H_2O+HOC^+$, and analogous deuterated reactions. The trajectory study shows that abstraction is the overwhelmingly dominant process in both systems, even though rearrangement to form the formyl cation is the energetically favored product in the case of $HF+HOC^+$ collisions. It might be inferred that entropic factors are dominant over enthalpic factors. More simply, we might say that the abstraction reaction can occur in a straightforward or direct manner that does not involve complicated molecular rearrangements in the ion–molecule complex. For both systems, abstraction appears to occur early in the reaction path so that the ion–molecule complex is not always formed for $HF+HOC^+$ collisions, and only rarely formed in $H_2O+HOC^+$ collisions.

## ACKNOWLEDGMENTS

The authors would like to thank Dr. Andrew Chalk for helpful contributions in the early stages of this work. We gratefully acknowledge a generous allocation of computer time from the Australian National University Supercomputer Facility and the support of the Australian Partnership for Advanced Computing.

[1] R. H. Nobes and L. Radom, Chem. Phys. **60**, 1 (1981).
[2] J. E. Del Bene, M. J. Frisch, K. Raghavachari, and J. A. Pople, J. Phys. Chem. **86**, 1529 (1982).
[3] D. A. Dixon, A. Komornicki, and W. P. Kraemer, J. Chem. Phys. **81**, 3603 (1984).
[4] D. J. DeFrees and A. D. McLean, J. Comput. Chem. **7**, 321 (1986).
[5] N. L. Ma, B. J. Smith, J. A. Pople, and L. Radom, J. Am. Chem. Soc. **113**, 7903 (1991).
[6] N. L. Ma, B. J. Smith, and L. Radom, Chem. Phys. Lett. **197**, 573 (1992).
[7] Y. Yamaguchi, C. A. Richards, and H. F. Schaefer, J. Chem. Phys. **101**, 8945 (1995).
[8] P. W. Harland, N. D. Kim, and S. A. H. Petrie, Aust. J. Chem. **42**, 9 (1989).
[9] S. G. Lias, J. E. Bartmess, J. F. Liebman, J. L. Holmes, R. D. Levin, and W. G. Mallard, J. Phys. Chem. Ref. Data Suppl. **17**, 1 (1988).
[10] C. G. Freeman, J. S. Knight, J. G. Love, and M. J. McEwan, Int. J. Mass Spectrom. Ion Processes **80**, 255 (1987).
[11] A. Cunje, C. F. Rodriguez, D. K. Bohme, and A. C. Hopkinson, J. Phys. Chem. A **102**, 478 (1988).
[12] R. C. Woods, R. J. Saykally, T. G. Anderson, T. A. Dixon, and P. G. Szanto, J. Chem. Phys. **75**, 4256 (1981).
[13] C. S. Gudeman and R. C. Woods, Phys. Rev. Lett. **48**, 1344 (1982).
[14] W. Wagner-Redeker, P. R. Kemper, M. F. Jarrold, and M. T. Bowers, J. Chem. Phys. **83**, 1121 (1985).
[15] R. C. Woods, C. S. Gudeman, R. L. Dickman, P. F. Goldsmith, G. R. Huguenin, W. M. Irvine, A. Hjalmarson, L.-A. Nyman, and H. Olofsson, Astrophys. J. **270**, 583 (1983).
[16] L. M. Ziurys and A. J. Apponi, Astrophys. J. Lett. **455**, L73 (1995).
[17] D. Buhl and L. E. Snyder, Nature (London) **228**, 267 (1970).
[18] A. J. Chalk and L. Radom, J. Am. Chem. Soc. **119**, 7573 (1997).
[19] D. K. Bohme, Int. J. Mass Spectrom. Ion Processes **115**, 95 (1992).
[20] A. J. Chalk and L. Radom, J. Am. Chem. Soc. **121**, 1574 (1999).
[21] M. A. Collins, S. Petrie, A. J. Chalk, and L. Radom, J. Chem. Phys. **112**, 6625 (2000).
[22] J. Ischtwan and M. A. Collins, J. Chem. Phys. **100**, 8080 (1994).
[23] M. J. T. Jordan, K. C. Thompson, and M. A. Collins, J. Chem. Phys. **102**, 5647 (1995).
[24] M. J. T. Jordan, K. C. Thompson, and M. A. Collins, J. Chem. Phys. **103**, 9669 (1995).
[25] M. J. T. Jordan and M. A. Collins, J. Chem. Phys. **104**, 4600 (1996).
[26] K. C. Thompson and M. A. Collins, J. Chem. Soc., Faraday Trans. **93**, 871 (1997).
[27] R. P. A. Bettens and M. A. Collins, J. Chem. Phys. **111**, 816 (1999).
[28] K. Song and M. A. Collins, Chem. Phys. Lett. **335**, 481 (2001).
[29] M. J. Frisch, G. W. Trucks, H. B. Schlegel *et al.* GAUSSIAN 94, Revision A.I., Gaussian, Inc., Pittsburgh, PA, 1995.
[30] G. W. Frisch, G. W. Trucks, H. B. Schlegel *et al.* GAUSSIAN 98, Revision A.6, Gaussian, Inc., Pittsburgh, PA, 1998.
[31] K. C. Thompson, M. J. T. Jordan, and M. A. Collins, J. Chem. Phys. **108**, 8302 (1998).
[32] M. A. Collins, Theor. Chem. Acc. **108**, 313 (2002).
[33] M. P. Allen and D. J. Tildesley, *Computer Simulations of Liquids* (Clarendon, Oxford, 1987), p. 146.
[34] H. W. Schranz, S. Nordholm, and G. Nyman, J. Chem. Phys. **94**, 1487 (1991).
[35] R. P. A. Bettens and M. A. Collins, J. Chem. Phys. **108**, 2424 (1998).
[36] R. P. A. Bettens and M. A. Collins, J. Chem. Phys. **109**, 9728 (1998).
[37] R. P. A. Bettens, T. Hansen, and M. A. Collins, J. Chem. Phys. **111**, 6322 (1999).
[38] M. A. Collins and D. H. Zhang, J. Chem. Phys. **111**, 9924 (1999).

This article is copyrighted as indicated in the article. Reuse of AIP content is subject to the terms at: http://scitation.aip.org/termsconditions. Downloaded to IP: 130.56.106.27 On: Mon, 12 Oct 2015 04:33:38